

Transport of particles by magnetic forces and cellular blood flow in a model microvessel

J. B. Freund and B. Shapiro

Citation: *Phys. Fluids* **24**, 051904 (2012); doi: 10.1063/1.4718752

View online: <http://dx.doi.org/10.1063/1.4718752>

View Table of Contents: <http://pof.aip.org/resource/1/PHFLE6/v24/i5>

Published by the [American Institute of Physics](#).

Related Articles

Reducing the data: Analysis of the role of vascular geometry on blood flow patterns in curved vessels
Phys. Fluids **24**, 031902 (2012)

Dynamics of microcapsules in oscillating shear flow
Phys. Fluids **23**, 111901 (2011)

Pair collisions of fluid-filled elastic capsules in shear flow: Effects of membrane properties and polymer additives
Phys. Fluids **22**, 123103 (2010)

Natural constructal emergence of vascular design with turbulent flow
J. Appl. Phys. **107**, 114901 (2010)

A rapid method to estimate Westergren sedimentation rates
Rev. Sci. Instrum. **80**, 096102 (2009)

Additional information on *Phys. Fluids*

Journal Homepage: <http://pof.aip.org/>

Journal Information: http://pof.aip.org/about/about_the_journal

Top downloads: http://pof.aip.org/features/most_downloaded

Information for Authors: <http://pof.aip.org/authors>

ADVERTISEMENT



**Running in Circles Looking
for the Best Science Job?**

Search hundreds of exciting
new jobs each month!

<http://careers.physicstoday.org/jobs>

physicstodayJOBS



Transport of particles by magnetic forces and cellular blood flow in a model microvessel

J. B. Freund^{1,a)} and B. Shapiro^{2,b)}

¹*Mechanical Science & Engineering and Aerospace Engineering, University of Illinois at Urbana-Champaign, 1206 West Green Street MC-244, Urbana, Illinois 61801, USA*

²*Aerospace Engineering, University of Maryland, 3178 Glenn L. Martin Hall, College Park, Maryland 20742, USA*

(Received 21 December 2011; accepted 19 April 2012; published online 29 May 2012)

The transport of particles (diameter $0.56 \mu\text{m}$) by magnetic forces in a small blood vessel (diameter $D = 16.9 \mu\text{m}$, mean velocity $U = 2.89 \text{ mm/s}$, red cell volume fraction $H_c = 0.22$) is studied using a simulation model that explicitly includes hydrodynamic interactions with realistically deformable red blood cells. A biomedical application of such a system is targeted drug or hyperthermia delivery, for which transport to the vessel wall is essential for localizing therapy. In the absence of magnetic forces, it is seen that interactions with the unsteadily flowing red cells cause lateral particle velocity fluctuations with an approximately normal distribution with variance $\sigma = 140 \mu\text{m/s}$. The resulting dispersion is over 100 times faster than expected for Brownian diffusion, which we neglect. Magnetic forces relative to the drag force on a hypothetically fixed particle at the vessel center are selected to range from $\Psi = 0.006$ to 0.204 . The stronger forces quickly drive the magnetic particles to the vessel wall, though in this case the red cells impede margination; for weaker forces, many of the particles are margined more quickly than might be predicted for a homogeneous fluid by the apparently chaotic stirring induced by the motions of the red cells. A corresponding non-dimensional parameter Ψ' , which is based on the characteristic fluctuation velocity σ rather than the centerline velocity, explains the switch-over between these behaviors. Forces that are applied parallel to the vessel are seen to have a surprisingly strong effect due to the streamwise-asymmetric orientation of the flowing blood cells. In essence, the cells act as low-Reynolds number analogs of turning vanes, causing streamwise accelerated particles to be directed toward the vessel center and streamwise decelerated particles to be directed toward the vessel wall. © 2012 American Institute of Physics. [<http://dx.doi.org/10.1063/1.4718752>]

I. INTRODUCTION

Ferromagnetic nanometer-scale particles are biomedically attractive for targeted delivery of drugs (e.g., chemotherapy) or therapeutic heating (hyperthermia).¹ Such particles can sometimes be injected locally to treat a downstream disease location (e.g., a tumor), but a more versatile application is to introduce them intravenously and then collect them to a target by an externally applied magnetic field. A permanent magnet can be used to collect particles near the surface, as was first suggested over 30 years ago.² The depth of the treatable region, which, for example, determines the deepest tumors that can be accessed, is set by the applied magnetic forces, which hold the particles in place against the blood flow. In recent years, novel multifunctional coatings and high magnetic moment particles have broadened the range of potential therapeutic applications,³ as have means of using

a) jbfreund@illinois.edu.

b) benshap@umd.edu.

magnetic resonance imaging (MRI) or MRI-like technology to steer particles to particular internal targets.^{4,5}

Advection-diffusion models for the transport and capture of magnetic particles have shown general agreement with experiments;^{6,7} we here focus on the complex of the interactions of the particles with flowing blood cells. In capillaries and the smallest venules and arterioles, the cellular character of blood is an essential factor leading to its widely known non-Newtonian character.⁸ Interactions with blood cells are also anticipated to be of importance for particle transport in small vessels.

The magnetic particles of interest here are on the same scale or smaller than platelets, and observations of platelet transport might therefore be relevant. Platelet-sized particles have been shown to be margined in vessels via interactions with blood cells,^{9,10} though their rate of diffusion appears to significantly decrease near vessel walls,¹¹ presumably because of the well-known near-wall cell-depleted region. Based upon this, we can anticipate that the magnetic particles might preferentially collect near to the vessel wall even in absence of magnetic forces. Thus, cell-enhanced diffusion should significantly reduce the requisite magnetic field strength well below what might be expected based upon relatively simple homogeneous fluid diffusive transport models, though external forces might still be important for the final stage of crossing the cell-free zone to the vessel wall. In the present study, we will consider both weak magnetic forces, where red cell-induced diffusive-like transport dominates magnetically forced transport, as well as magnetic forces strong enough to dominate the motion of the particles. In all cases considered, even in absence of applied forces, the effective diffusion caused by cellular interactions is expected to be 100 times faster than thermal Brownian diffusion, which is therefore neglected (see Sec. II A).

Given the approximate streamwise symmetry of a blood vessel, it might not be anticipated that the streamwise component of the magnetic force will have any substantial effect. However, flowing red cells have a streamwise asymmetric^{12,13} structure, which has the potential to break this symmetry. We shall see that such a force can indeed alter the particle interactions with blood cells in an asymmetric fashion, even when it is so weak that its effect on particle residence times is small.

We investigate these issues in a model geometry that includes realistically flexible flowing red cells. Section II summarizes the flow parameters, the physical model, the algorithm used to numerically solve the flow, and the simulation procedure. Results are discussed in Sec. III for cellular transport of particles without magnetic forces, for increasing cross-stream magnetic forces, and for a range of magnetic force strengths parallel and counter-parallel to the flow direction.

II. SIMULATION MODEL

A. Flow parameters

The round-tube model of a small blood vessel is shown in Figure 1 [see Video 1 for an animation of the subsequent flow]. It is streamwise periodic to model a longer tube than could be efficiently simulated directly. For a red cell with volume $4\pi a_o^3/3 = 93.94 \mu\text{m}^3$, the vessel diameter is $D = 6a_o = 16.9 \mu\text{m}$ and its length is $L_z = 12.7a_o = 33.9 \mu\text{m}$. There are 19 red cells included in the simulation, which yields a mean tube hematocrit (red cell volume fraction) of $H_c = 0.22$. The mean velocity in all cases is $U = 2.89 \text{ mm/s}$, which corresponds to a physiologically relevant⁸ pseudo-shear rate of $UID = 171 \text{ s}^{-1}$.

Ten magnetic particles are modeled as rigid spheres, each with radius of $a_p = 0.1a_o = 0.282 \mu\text{m}$ and hence 1000th the red cell volume. Based upon an Einstein estimate of the thermal diffusion of a sphere in a fluid with the plasma viscosity ($\approx 5 \times 10^{-14} \text{ m}^2/\text{s}$), the average arrival time for such particles released at the vessel center to reach the wall would be around 500 s in absence of cellular interactions. Since this far exceeds the time of the particle transport we shall see due to the unsteady motions of the cells, we neglect all such Brownian diffusion in our study of transport toward the wall, though it will undoubtedly become important in the final stages before actual wall contact.

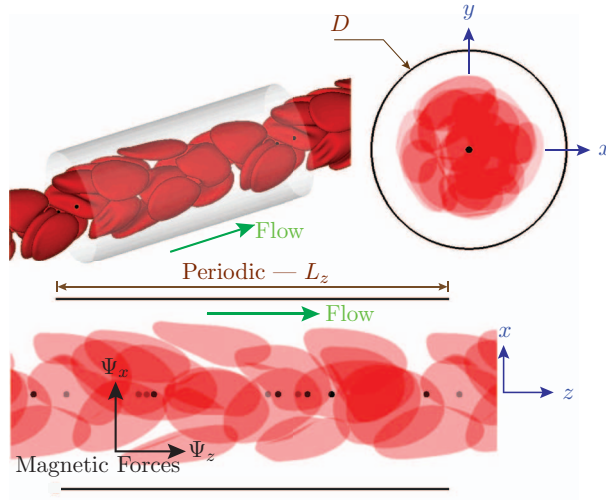


FIG. 1. Visualization of the initial condition showing the red cells and magnetic particles (enhanced online) [URL: <http://dx.doi.org/10.1063/1.4718752.1>].

The strength of the magnetic force relative to a hypothetical vessel centerline hydrodynamic drag is

$$\Psi = \frac{\text{magnetic force}}{\text{Stokes drag for centerline velocity}} = \frac{\mathbf{F}}{6\pi\mu_b a_p V_c} = \frac{\mathbf{V}_R}{V_c}, \quad (1)$$

where \mathbf{V}_R is the (vector) velocity that would be induced by the applied magnetic force on an isolated particle in a homogeneous Newtonian fluid with viscosity μ_b . For $H_c = 0.22$, μ_b is approximately twice the plasma viscosity, so we take $\mu_b = 2\mu = 0.0024$ Pa s.¹⁴ This non-dimensional force Ψ has been shown significant in magnetic particle capture¹⁵ and has been termed a magnetic Richardson number.⁷ Any magnetic shielding effects are neglected so the magnetic field is assumed to apply identical forces to each particle. The centerline velocity is $V_c = 4.6$ mm/s in all cases (see Sec. III A). Of the components of $\Psi = (\Psi_x, \Psi_y, \Psi_z)$, we will focus primarily on Ψ_x , which forces the magnetic particles perpendicular to the flow direction. It will be varied from $\Psi_x = 0$ to 0.204. Symmetry indicates that negative Ψ_x or finite Ψ_y would not yield statistically different behavior from the $\Psi_x \geq 0$ and $\Psi_y = 0$ cases considered. We also consider finite Ψ_z from $\Psi_z = -0.204$ to 0.204 along the axis of the tube. For reference, $\Psi_z = -1$ should hold the particle in place against the drag force exerted by the flow of homogeneous fluid with viscosity μ_b . The actual forces range up to 2.9pN per particle. Specific parameters for specific cases will be discussed in Sec. III.

The red cells are modeled as fluid filled elastic shells, which resist both bending and in-plane shear. It is thought that the interior viscosity of a red cell is several times that of the suspending plasma,¹⁶ with a factor of $\lambda = 5$ a common choice in models,¹⁷ but detailed simulation studies have also shown that the basic flow of red cells in small vessels is relatively insensitive to this.¹³ The particular solver we use (Sec. II B) is more efficient for cell interior and plasma viscosities that match, so we use this as a model in the present study. The specific parameters used in the neo-Hookean elastic model for the shell-membrane stresses are those of Pozrikidis,¹⁷ which are based upon experimental measurements: shear modulus $E_s = 4.2 \times 10^{-6}$ N/m and bending modulus $E_b = 1.8 \times 10^{-19}$ N m. Red cells are well known to have a nearly constant membrane area, which is modeled here with a large penalty-like dilatation modulus: $E_d = 67.7 \times 10^{-6}$ N/m. This model is, in a sense, crude in that red cell membranes will require a more complex constitutive model to reproduce behavior in many conceivable situations. However, it has matched the non-monotonic effective viscosity measurements for flow in round tubes ranging from $D = 5 \mu\text{m}$ up to $D = 28 \mu\text{m}$.^{18,19} The same flow regime is studied herein, so the model is therefore expected to

perform well. We also neglect in-membrane viscosity, which is large and has not been shown to be important for flows such as we consider, though it too undoubtedly becomes important in some circumstances.

B. Flow solver

For the low Reynolds numbers of the microcirculation (here $\rho U D / \mu = 0.003$), the governing equations can be approximated by their viscous limit and crafted into a boundary integral formulation.²⁰ This is solved with the fast algorithm we have developed and reported in Refs. 18 and 19. In brief, the surface of each cell or magnetic particle is discretized with a two-dimensional structured mesh of surface elements, and the vessel wall is discretized with an unstructured surface mesh of 25 704 triangular elements. To evaluate the hydrodynamic interactions of all these N_p surface elements, the periodic-box Green's functions of the Stokes operator are split into close-range interactions, which are computed directly, and long-range interactions, which are evaluated using Fourier methods on a mesh. Our basic algorithm is similar to the particle-mesh-Ewald algorithm proposed for suspensions by Saintillan *et al.*²¹ The result is that the overall N_p^2 point-to-point interactions are computed with a computational cost that scales as $N_p \log N_p$. The force required to enforce the no-slip boundary condition is solved iteratively with a GMRES (Ref. 22) algorithm using a single-layer formulation.²⁰ The rigidity of the magnetic particles introduces an implicit system, which is also solved iteratively using GMRES. As crafted, this linear system is unsuited for iterative solution due to the eigenvalues associated with the rigid-body motions of the particles, so these corresponding eigenvectors are projected out of the linear system using an established deflation procedure before the iterative solution.^{20,23}

The elastic forces exerted by the cells on the fluid are evaluated using a spherical harmonic representation of the cell shape. This is advantageous in that a small number of degrees of freedom provide an accurate description of both the cell shape and the derivatives necessary to calculate the elastic stresses. It also facilitates numerical stability without the addition of artificial numerical dissipation. In the present study, a spherical harmonic expansion of maximal degree $N = 16$ for each coordinate component (x , y or z) represents each cell, which corresponds to N^2 degrees of freedom per component per cell. Nonlinear operations are performed on a finer surface mesh with a spherical harmonic expansion of maximum degree of $M = 3N$ to maintain stability via what amounts to an approximate de-aliasing procedure.^{18,19}

C. Simulation procedure

The common initial condition used for all the reported simulations is visualized in Figure 1. To generate it, the 19 red cells were simulated without magnetic particles for time $t \approx 100$ ms, which allowed 10 flow-throughs of the $L_z = 35.9 \mu\text{m}$ streamwise-periodic tube as shown. This was sufficiently long to establish an apparently random distribution of cells within the tube. At this point, the 10 magnetic particles were distributed along the tube centerline ($r = 0$) in positions vacant of red cells. The specific locations can be seen in Figure 1. For the cases with magnetic fields, these forces were initiated immediately. Particle positions as well as the shapes and positions of all the red cells were tracked in time.

III. RESULTS

A. Red-cell flow statistics

The mean velocity profile in small blood vessels is well known to be blunted, significantly flatter than the Poiseuille-flow parabola for a constant viscosity homogeneous Newtonian fluid. Long,²⁴ for example, shows this clearly in vessels down to $D = 24 \mu\text{m}$. We do not attempt to replicate any particular set of experimentally studied flow parameters, but the flowing cells in the present case show this expected blunting in Figure 2. The parabolic velocity profile for the corresponding plasma-viscosity Poiseuille flow is also shown for comparison. Our past validation against measured effective viscosities suggest that the overall rheology is quantitatively realistic.^{18,19} Given the relatively small

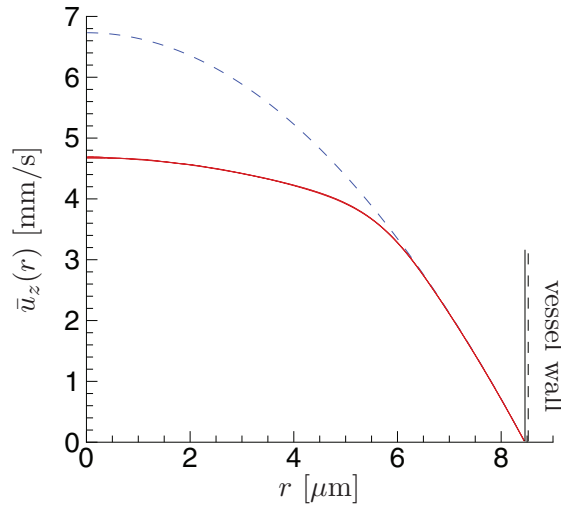


FIG. 2. Mean velocity versus $r = \sqrt{x^2 + y^2}$: — simulations and - - - the corresponding Poiseuille-flow for the same pressure gradient. The simulation results show overlaying results for three cases: $\Psi = (0, 0, 0)$, $(0, 0, 0.1)$, and $(0, 0, -0.1)$.

size of the magnetic particles, we would not expect any significant effect on the flow, which is confirmed in Figure 2. Even when the magnetic forces are aligned parallel with the flow direction mean-flow profiles still overlay one another on the plot.

Red cells are also known to deform significantly under physiologic flow conditions, as is clear in Figure 1. In the smallest vessels, where they are constrained to flow in a single file, they become bullet-shaped; in slightly larger vessels they take on what is sometimes called a slipper-like shape. We shall see that their orientation, particularly their streamwise asymmetry, is an important factor in the transport of the magnetic particles.

To quantify cell orientation, we use a metric based upon the principal axes of the cell shapes, which can be used to generate fitted ellipsoids. This follows the same formulation of our previous study,¹³ so here we only summarize it. The ellipsoids are constructed from the eigenvectors of

$$M_{ij} = \frac{1}{A} \int_A x'_i x'_j dS(\mathbf{x}), \quad (2)$$

where A is the cell surface and \mathbf{x}' is a surface coordinate measured relative to the cell centroid: $\mathbf{x}' = \mathbf{x} - \mathbf{x}_c$. These eigenvectors \mathbf{e}_1 , \mathbf{e}_2 , and \mathbf{e}_3 , which have corresponding eigenvalues $\lambda_1 > \lambda_2 > \lambda_3$, can be used to construct a fitted ellipsoid as

$$\mathbf{x} = 2\sqrt{\lambda_1}\mathbf{e}_1 \sin \psi \cos \varphi + 2\sqrt{\lambda_2}\mathbf{e}_2 \cos \psi \cos \varphi + 2\sqrt{\lambda_3}\mathbf{e}_3 \sin \varphi, \quad (3)$$

where $\psi \in [0, \pi]$ and $\varphi \in [0, 2\pi]$. These are shown in Figure 3(a). We define tilt angle θ for each cell as the angle between its shortest axis and the inward directed normal to the tube wall closest to the cell centroid, as shown in Figure 3(b). Based upon the visualizations, we expect typical θ , defined in this way, to be negative. This is almost always true, as seen in Figure 3(c), which shows the angle probability density function $\mathcal{P}(\theta)$ normalized such that

$$\frac{1}{2\pi} \int_{-\pi}^{\pi} \mathcal{P}(\theta) d\theta = 1. \quad (4)$$

The nearly identical distribution for the several simulation cases plotted in Figure 3(c) confirms that the magnetic particles, even when subjected to the strongest forces studied, do not significantly affect red cell orientations.

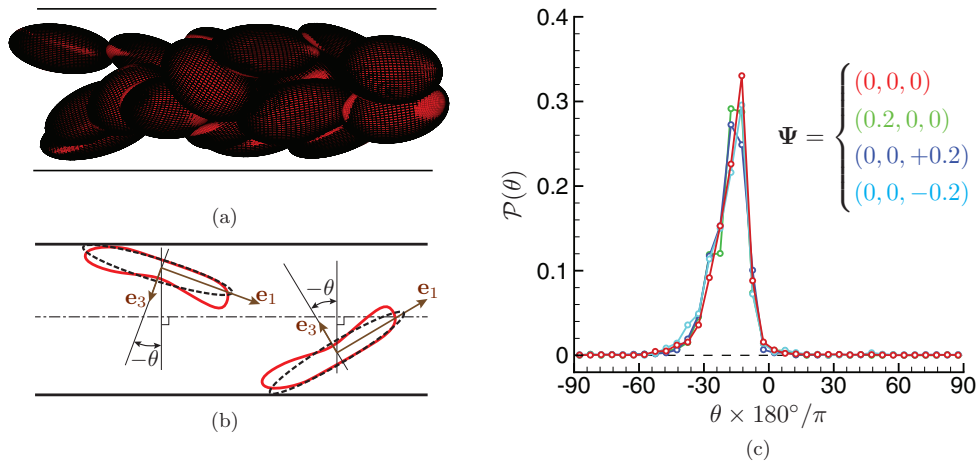


FIG. 3. (a) Red cells with their respective fitted ellipsoids. (b) The principal eigenvector e_3 associated with the smallest eigenvalue λ_3 is used to quantify the tilt angle of each cell. As shown, both cells have negative tilt angles. (c) The average distribution of tilt angles for the cases with the magnetic forces as labeled.

B. Force-free particle advection

Without applied magnetic forces, the particles are simply advected and are dispersed by the apparently chaotic motion of the red cells. Figure 4(a) shows the motion of the particles projected onto a x - y plane, and Figure 4(b) shows the time history of maximum distance of the particles (measured to the particle surface) from the tube centerline. We see that particles that reach the cell-free layer ($r \gtrsim 6 \mu\text{m}$) tend to stay there, which suggests that they will, in time, become concentrated near the vessel wall, as has been observed for platelets.²⁵ This is consistent with recent observations showing small effective diffusivity near the wall in an experimental study of passive particle transport.¹¹

The x -velocity distribution for particles with centers $r(t) = \sqrt{x^2(t) + y^2(t)} \leq 6 \mu\text{m}$, is shown in Figure 5. Though obviously important for lateral transport, no fluctuation exceeds 10% of the centerline velocity ($\bar{u}_z(0) = 4.6 \text{ mm/s}$). The statistics are approximately Gaussian, reasonably well fitted by $\mathcal{P}(v_x) \propto \exp[-v_x^2/2\sigma^2]$ with $\sigma = 140 \mu\text{m/s}$. The velocity in just the x coordinate direction

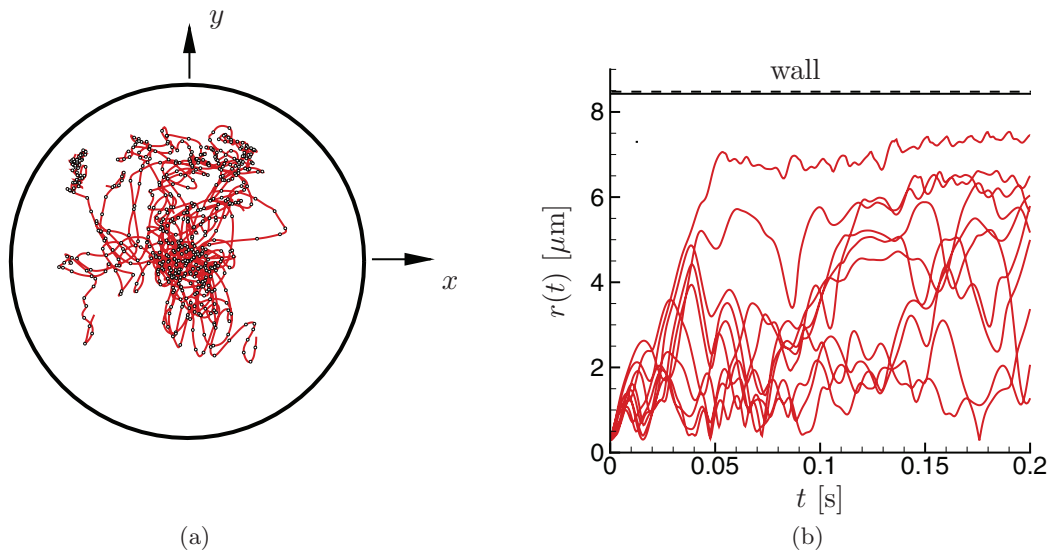


FIG. 4. Particles trajectories without magnetic forces: (a) projected onto a x - y plane and (b) maximum instantaneous distance from the tube centerline $r(t) = \sqrt{x^2(t) + y^2(t)}$.

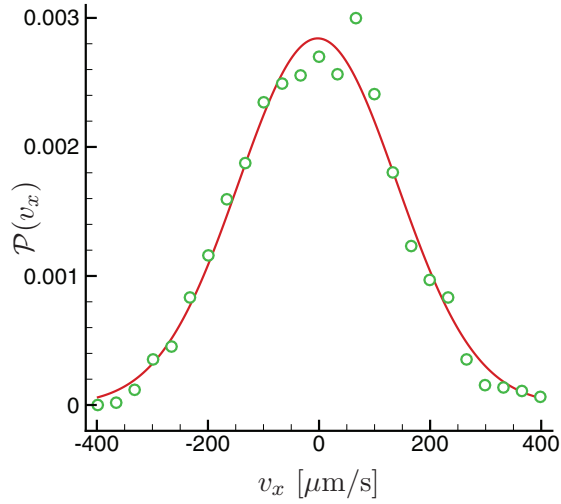


FIG. 5. Probability density function ($\int_{-\infty}^{\infty} \mathcal{P}(v_x) dv_x = 1 \mu\text{m/s}$) of x velocity for particles with $r(t) \leq 6 \mu\text{m}$ averaged over the period of the simulation. The symbols \circ correspond to data accumulated in bins from the simulation data and the line — is a Gaussian fit (see text).

was selected over the radial velocity to remove the effect of the mean drift toward the periphery of the vessel in this transient simulation. However, the radial velocity distribution is almost indistinguishable. The corresponding distribution of radial velocity is least-squares fitted with nearly the same width Gaussian ($\sigma = 138 \mu\text{m/s}$) except that its fit $\exp[-(v_r - v_o)^2/2\sigma^2]$ is centered at $v_o = 32 \mu\text{m/s}$, reflecting the relatively slow mean outward drift of the particles. An effective net radial diffusivity can be deduced from the time it takes, say, half the particles to reach the cell-free layer at $r \approx 6 \mu\text{m}$. From Figure 4(b), we see that this corresponds to $t \approx 0.25\text{s}$, which is consistent with an effective radial diffusivity of $D \approx 5 \times 10^{-11} \text{m}^2/\text{s}$. This is similar to the diffusivities ($D \approx 4 \times 10^{-11} \text{m}^2/\text{s}$) of small beads and platelets recently computed and compared favorably with experiments by Zhao and Shaqfeh.²⁵

Since these velocity fluctuations also transport the magnetic particles, how they compare with the induced velocity of any applied magnetic force is also important. We thus define the fluctuation-velocity analog of Ψ from (1) as

$$\Psi' = \frac{\text{magnetic force}}{\text{Stokes drag for fluctuation velocity}} = \frac{\mathbf{F}}{6\pi\mu a_p \sigma} = \frac{\mathbf{V}_R}{\sigma}. \quad (5)$$

For the parameters studied here, components of Ψ' will range in magnitude from 0 to 6.70, thus spanning between $|\Psi'| > 1$ and $|\Psi'| < 1$ regimes where magnetic forces will be, respectively, large and small compared to the fluctuation velocity drag forces. We can anticipate that Ψ' will thus be an indicator of behavior regime based upon the magnetic force strength.

The therapeutic objective requires that the particles reach the vessel wall. Though interactions with the red cells also push the particles toward the near-wall cell-free layer, upon reaching it they persist for long periods at the edge of this layer. As expected for viscous flow, there do not seem to be any significant hydrodynamic forces causing further wall-ward motion upon entering this cell-free layer, only a slow drift toward the wall (see Figure 4(b)) as would be expected to arise via the weak nonlinearity associated with small deformations of nearby blood cells.²⁵ For drug delivery, this persistence might be beneficial since it inhibits the absorption of particles except where a magnetic force is applied in a way to accelerate the final transport to the vessel wall. We next consider such a force.

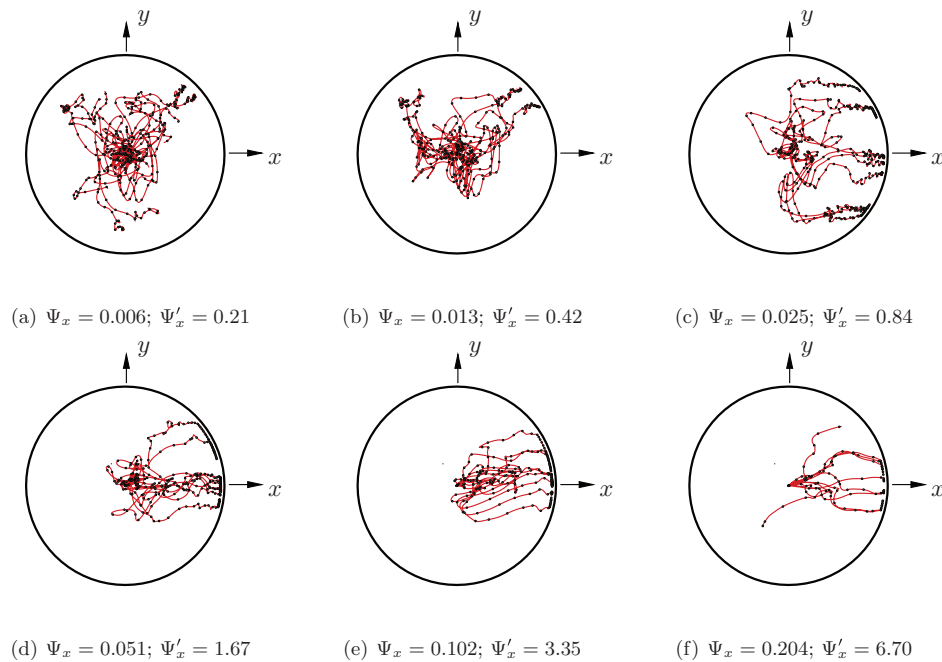


FIG. 6. Particle trajectories for increasing Ψ_x as labeled. The corresponding $\Psi_x = 0$ case is shown in Figure 4(a).

C. Magnetic forces perpendicular to the flow direction

Figure 6 shows the particle trajectories for x -directed forces that range from $\Psi_x = 0.006$ up to $\Psi_x = 0.204$. It is clear that the weaker forces are insufficient to resist the diffusional buffeting of the red cells, which obviously dominates their motion. However, with increasing Ψ_x there is a clear x -direction bias to their trajectory, with the strongest force yielding a fast, and for most particles monotonic, approach toward the vessel wall. A key difference from the $\Psi_x = 0$ case is that even a relatively weak force will be significant once the particles reach the near-wall cell-free layer. We see continued transport toward the wall in all cases.

The corresponding Ψ'_x are also labeled in Figure 6. For $\Psi'_x > 1$, we see a clear and immediate motion in the $+x$ -direction. For the highest Ψ'_x , the particles almost all reach the the cell-free region and wall near $y \approx 0$ where the particles were released, indicating that the magnetic forces overwhelm the lateral dispersion caused by interactions with the red cells. When $\Psi'_x \approx 1$, in Figure 6(c), there is an obvious trend of magnetic particle motion in the $+x$ direction, but it is wandering and there is also significant lateral dispersion in the $\pm y$ -directions. For still smaller Ψ'_x , the fluctuations dominate the magnetic force and the motion looks superficially like that without an applied magnetic force.

In Figure 7, which shows the distance of the particles from the vessel center, we confirm that a transition of sorts occurs at $\Psi'_x \approx 1$. For $\Psi'_x > 2$, most of the particles move toward the wall at approximately the velocity predicted for an isolated sphere in a fluid with the plasma viscosity. Some of the particles are impeded temporarily by interactions with cells, but this is a small number (only two for the largest $\Psi_x = 0.2$ case). If it were assumed that the particles were suspended in a homogeneous fluid with the bulk blood viscosity μ_b , in this strong-force limit many of the particles would appear to arrive even sooner than expected (Figures 7(d)–7(f)). Most that show any obvious interactions with the cells are only temporarily delayed, with the result that their wall arrival time roughly corresponds to that predicted for homogeneous fluid with the blood viscosity.

For $\Psi'_x \lesssim 1$, however, the particle interactions with the red cells dominate the transport. Most particles actually reach the edge of the cell-free layer before they would have in absence of red cells, as estimated by the free-space velocity prediction, especially if an effective μ_b were used for the

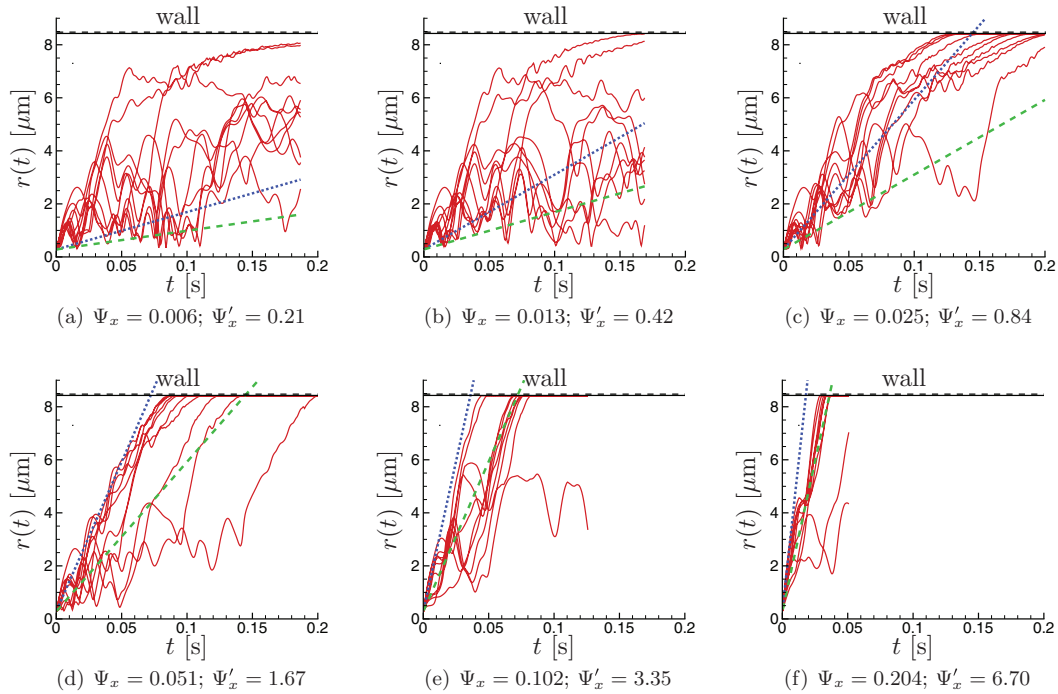


FIG. 7. Particle radial location histories for increasing Ψ_x as labeled: — simulated particles and predictions for a sphere in unbounded fluid with the plasma viscosity μ ····· and bulk blood viscosity μ_b - - - - .

viscosity. The magnetic field then moves them toward the wall. Note that lateral dispersions lead to some of these particles entering the cell-free layer well away from $y = 0$, as seen, for example, in Figure 6(c). Thus, even if they were to move at the free-space velocity, they would appear to approach the wall more slowly because the magnetic forces are not directed toward the closest part of the vessel wall. The resulting trajectories are seen in Figure 7(c). Even magnetic fields that are too weak to significantly affect transport in the cell-rich core become important once the particles reach the cell free layer.

D. Magnetic forces parallel to the flow direction

Though forces perpendicular to the flow are the most intuitive for bringing the particles to the vessel walls, we should also consider forces with a finite streamwise component since a vascular system will have a range of vessel orientations. Indeed, forces oriented predominantly perpendicular to the flow are expected to be rare. For a homogeneous fluid, the effect of a streamwise component would be simple: only if it significantly increases residence time will it then allow a flow-perpendicular force component to increase transport to the vessel wall. However, for $|\Psi| \ll 1$ this effect will be small, since such small magnetic forces do not significantly affect residence times. However, we shall see that the particular inhomogeneous environment established by the sheared red cells amplifies the effect of streamwise oriented forces.

Figure 8 shows the particle $r(t)$ histories for a range of positive and negative Ψ_z . The corresponding case with $\Psi = 0$ was shown in Figure 4(b). Forces in the flow direction ($\Psi_z > 0$) clearly suppress the radial transport of the particles whereas forces counter to the flow ($\Psi_z < 0$) clearly promote it. This is due to the streamwise asymmetry of the blood cells. As seen in the visualization (Figure 1) and confirmed quantitatively based upon the orientation of fitted ellipsoids (Figure 3), the cells flow with orientation such that their leading edge is tilted toward the center of the vessel. As shown schematically in Figure 9, a particle that is decelerated relative to the local flow will encounter the typical cell in a way that directs it toward the vessel wall. In contrast, a particle that is accelerated relative to the flow has the opposite tendency. In short, the cells act as

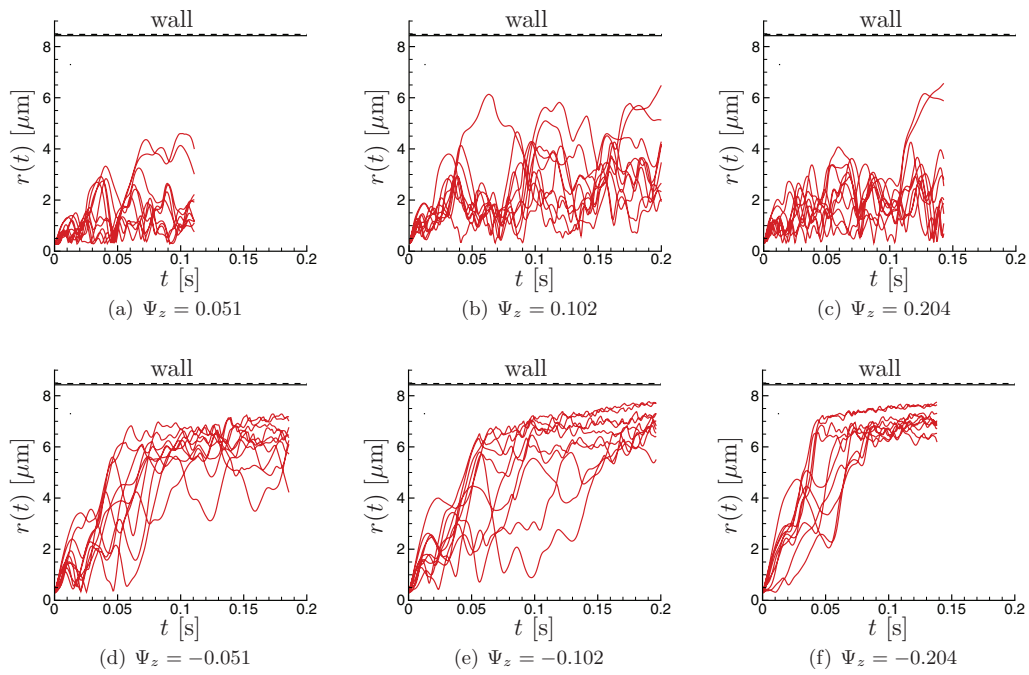


FIG. 8. Particle radial location histories for $\Psi_x = 0$ and the Ψ_z as labeled.

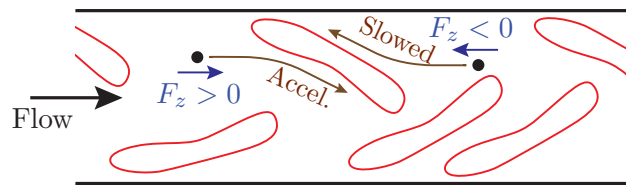


FIG. 9. The asymmetry of the cells directs the particles toward or away from the wall depending upon the sense of the force relative to the flow direction.

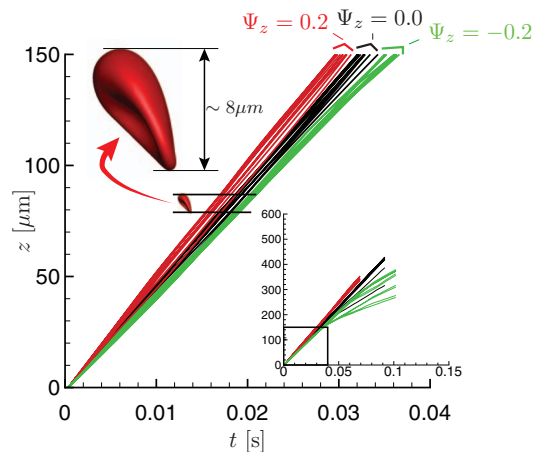


FIG. 10. Travel distance for $\Psi = (0, 0, 0.2)$, $(0, 0, 0)$, and $(0, 0, -0.2)$ cases as labeled.

a zero-Reynolds number analog of turning vanes, greatly enhancing any effect of the streamwise force.

For the mechanism suggested in Figure 9, we expect to see a significant effect when the force has moved the particle approximately a cell length relative to a nearby flowing cell. This is quantified in Figure 10. The relative streamwise motion caused by streamwise versus counter-stream force is approximately cell scale ($\sim 8 \mu\text{m}$) after about time 0.02s. This can be anticipated based upon the $\Psi_z = -0.204$ case. In a homogeneous fluid of plasma viscosity, the particle would move about $8 \mu\text{m}$ relative to the plasma in about 0.05s. This corresponds to the margination time for $\Psi_z = -0.204$ seen in Figure 8(f), which precipitates a significant divergence in the trajectories (inset of Figure 10) as particles in the $\Psi_z = -0.204$ case arrive in the slow-flowing fluid near the vessel wall (Figure 8(f)).

IV. SUMMARY AND CONCLUSIONS

In summary, we see significant influence of the cellular character of the blood upon the transport of the magnetic particles. Without any forces applied, the particles have root-mean-square velocity fluctuations perpendicular to the mean that are nearly 5% of the mean flow $\langle v_x^2 \rangle^{1/2} = 0.045U = 140 \mu\text{m/s}$. In flows with relatively weak cross-stream magnetic forces, particularly those with $\Psi'_x \lesssim 1$, these fluctuations accelerate the particle transport toward the wall, which could lead to contact more quickly than a free-space Stokes-law would predict. Even relatively weak forces can be significant in the near-wall cell-free layer, which the particles must traverse to reach the wall. Upon entering this region, there are no longer strong interactions with the cells to promote wall-ward dispersion. Brownian motion would also have more time to act in this region, becoming significant for any particles as they near the vessel, especially for those smaller than the $a_b = 0.282 \mu\text{m}$ radius considered here. This might be particularly important since preferential margination would necessarily cease in the small particle limit, where they become passive zero-dimensional flow tracers. Preferential margination as we see through interaction with red cells depends upon their finite size. For stronger forces ($\Psi'_x \gtrsim 1$), interactions with the cells inhibit contact with the wall but does not slow transport by more than a factor of two for most particles.

The effect of streamwise-directed magnetic fields was surprisingly significant. The asymmetric orientation of the cells caused them to act similar to turning vanes, directing the particles toward the vessel center for magnetic forces in the flow direction and toward the vessel wall for forces counter to the flow direction. This is a much more significant effect than might be anticipated based upon the simple change in residence time: it occurs on the time it takes for a particle to pass or be passed by a red cell in the flow. This has not apparently been observed yet in blood cell experiments, but it is a potentially useful means of altering transport. This effect is expected to diminish and eventually disappear in the smallest vessels, where the cells flow in single file in a nearly axisymmetric shape. Also, for significantly larger vessels, cells further from the vessels walls are not expected to flow with so consistent a vane-like orientation. Vessel-size dependence is thus worthy of further investigation.

ACKNOWLEDGMENTS

Support from National Science Foundation (NSF) (CBET 09-32607) is gratefully acknowledged.

- ¹Q. A. Pankhurst, J. Connolly, S. K. Jones, and J. Dobson, "Applications of magnetic nanoparticles in biomedicine," *J. Phys. D* **36**, R167 (2003).
- ²K. Mosbach and U. Schroder, "Preparation and application of magnetic polymers for targeting of drugs," *FEBS Lett.* **102**, 112 (1979).
- ³Q. A. Pankhurst, N. K. T. Thanh, S. K. Jones, and J. Dobson, "Progress in applications of magnetic nanoparticles in biomedicine," *J. Phys. D* **42**, 224001 (2009).
- ⁴J.-B. Mathieu and S. Martel, "Magnetic microparticle steering within the constraints of an MRI system: Proof of concept of a novel targeting approach," *Biomed. Microdevices* **9**, 801–808 (2007).
- ⁵J. Riegler, J. A. Wells, P. G. Kyrtatos, A. N. Price, Q. A. Pankhurst, and M. F. Lythgoe, "Targeted magnetic delivery and tracking of cells using a magnetic resonance imaging system," *Biomaterials* **31**, 5366 (2010).
- ⁶C. F. Driscoll, R. M. Morris, A. E. Senyei, K. J. Widder, and G. S. Heller, "Magnetic targeting of microspheres in blood flow," *Microvasc. Res.* **27**, 353 (1984).

- ⁷ A. Nacev, C. Beni, O. Bruno, and B. Shapiro, "Magnetic nanoparticle transport within flowing blood and into surrounding tissue," *Nanomedicine* **5**, 1459 (2010).
- ⁸ A. R. Pries, D. Neuhaus, and P. Gaetgens, "Blood viscosity in tube flow: Dependence on diameter and hematocrit," *Am. J. Physiol. Heart Circ. Physiol.* **263**, H1770 (1992).
- ⁹ R. Zhao, M. V. Kameneva, and J. F. Antaki, "Investigation of platelet margination phenomena at elevated shear stress," *Biorheology* **44**, 161 (2007).
- ¹⁰ T. Karino and H. Goldsmith, "Aggregation of human platelets in an annular vortex distal to a tubular expansion," *Microvasc. Res.* **17**, 217 (1979).
- ¹¹ M. Saadatmand, T. Ishikawa, N. Matsuki, M. J. Abdekhodaie, Y. Imai, H. Ueno, and T. Yamaguchi, "Fluid particle diffusion through high-hematocrit blood flow within a capillary tube," *J. Biomech.* **44**, 170 (2011).
- ¹² P. Gaetgens, C. Dührssen, and K. H. Albrecht, "Deformation, and interaction of blood cells and plasma during flow through narrow capillary tubes," *Blood Cells* **6**, 799 (1980).
- ¹³ J. B. Freund and M. M. Orescanin, "Cellular flow in a small blood vessel," *J. Fluid Mech.* **671**, 466 (2011).
- ¹⁴ R. L. Whitmore, *Rheology of the Circulation* (Pergamon, Oxford, 1968).
- ¹⁵ A. Sinha, R. Ganguly, A. K. De, and I. K. Puri, "Single magnetic particle dynamics in a microchannel," *Phys. Fluids* **17**, 117102 (2007).
- ¹⁶ L. Dintenfuss, "Internal viscosity of the red cell and a blood viscosity equation," *Nature (London)* **219**, 956 (1968).
- ¹⁷ C. Pozrikidis, "Axisymmetric motion of a file of red blood cells through capillaries," *Phys. Fluids* **17**, 031503 (2005).
- ¹⁸ H. Zhao, A. H. G. Isfahani, L. Olson, and J. B. Freund, "A spectral boundary integral method for flowing blood cells," *J. Comput. Phys.* **229**, 3726 (2010).
- ¹⁹ J. B. Freund and H. Zhao, "A fast high-resolution boundary integral method for multiple interacting blood cells," in *Computational Hydrodynamics of Capsules and Biological Cells*, edited by C. Pozrikidis (CRC, Boca Raton, Florida, 2010), pp. 71–111.
- ²⁰ C. Pozrikidis, *Boundary Integral and Singularity Methods for Linearized Viscous Flow* (Cambridge University Press, Cambridge, 1992).
- ²¹ D. Saintillan, E. Darve, and E. S. G. Shaqfeh, "A smooth particle-mesh Ewald algorithm for Stokes suspension simulations: The sedimentation of fibers," *Phys. Fluids* **17**, 033301 (2005).
- ²² Y. Saad and M. H. Schultz, "GMRES: A generalized minimal residual algorithm for solveing nonsymmetric linear systems," *SIAM (Soc. Ind. Appl. Math.) J. Sci. Stat. Comput.* **7**, 856 (1986).
- ²³ S. Kim and S. J. Karrila, *Microhydrodynamics: Principles and Selected Applications* (Butterworth-Heinemann, Boston, 1991).
- ²⁴ D. S. Long, "Microviscometric analysis of microvascular hemodynamics in vivo," Ph.D. dissertation, University of Illinois at Urbana-Champaign, Urbana, Illinois, 2004.
- ²⁵ H. Zhao, E. S. G. Shaqfeh, and V. Narsimhan, "Shear-induced particle migration and margination in a cellular suspension," *Phys. Fluids* **24**, 011902 (2012).